DOI: 10.1111/tgis.12269

RESEARCH ARTICLE

WILEY Transactions in GIS

# Spheroidal equal angular DEMs: The specificity of morphometric treatment

Igor V. Florinsky

Institute of Mathematical Problems of Biology, Keldysh Institute of Applied Mathematics, Moscow Region, Russia

**Correspondence**
Institute of Mathematical Problems of Biology, Keldysh Institute of Applied Mathematics, Russian Academy of Sciences.1, Vitkevich St., Pushchino, Moscow Region, 142290, Russia.
Email: iflor@mail.ru

## Abstract

Digital elevation models (DEMs) are commonly constructed using two main types of regular grids: plane square grids and spheroidal equal angular grids. Methods and algorithms intended for plane square-gridded DEMs should not be directly applied to spheroidal equal angular DEMs. This is because these grids have fundamentally different geometry. However, some researchers continue to apply square-grid algorithms to spheroidal equal angular DEMs. It seems appropriate to consider once again the specifity of morphometric treatment of spheroidal equal angular DEMs. This article, first, demonstrates possibilities of direct calculation of local, nonlocal, and combined morphometric variables from spheroidal equal angular DEMs exemplified by slope gradient, catchment area, and topographic index. Second, the article shows computational errors when algorithms for plane square-gridded DEMs are unreasonably applied to spheroidal equal angular DEMs. The study is exemplified by two DEMs. A medium-resolution DEM of a relatively small, high-mountainous area (Mount Elbrus) was extracted from the SRTM1 DEM. A low-resolution DEM of a vast region with the diverse topography (the central and western regions of Kenya) was extracted from the SRTM30_PLUS DEM. The results show that application of square-grid methods to spheroidal equal angular DEMs leads to substantial computational errors in models of morphometric variables.

**KEYWORDS**
computation, Digital elevation model, error, grid, geomorphometry

## 1 | INTRODUCTION

Digital terrain analysis is widely used to solve various multiscale problems of geosciences, including landform and hydrological modelling, predictive soil and vegetation mapping, revealing and analysis of geological features, modelling of terrain evolution, terrain visualization, and so on (Moore, Grayson, & Ladson, 1991; Franklin, 1995; Wilson & Gallant, 2000; Li, Zhu, & Gold, 2005; Deng, 2007; Hengl & Reuter, 2009; Brocklehurst, 2010; Florinsky, 2012). One of the key

  

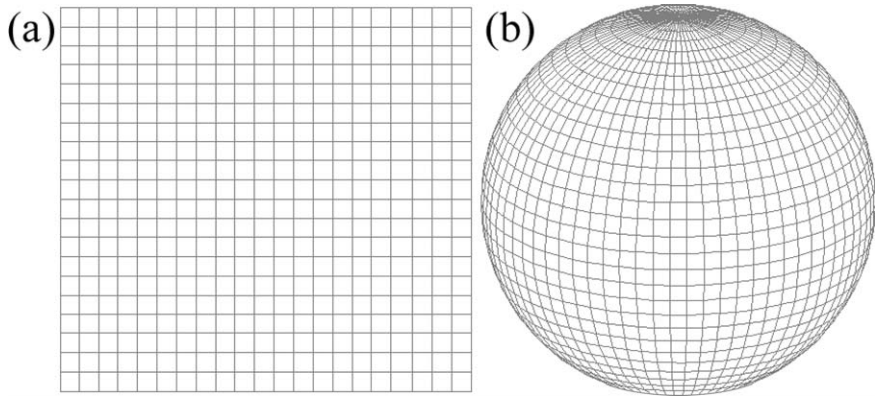


**FIGURE 1** Two types of regular grids of DEMs: (a) Plane square grid. (b) Spheroidal equal angular grid

steps and procedures of digital terrain analysis is derivation of digital models of morphometric variables from digital elevation models (DEMs).

It is well known that DEMs are commonly constructed by interpolation of raw elevation data using two main kinds of regular grids: (1) plane square grids, and (2) spheroidal equal angular grids (Figure 1). Grids of the first kind are typical for high- and medium-resolution DEMs of relatively small areas, when the curvature of a planet may be ignored. Grids of the second kind are employed to describe the topography of the globe or vast territories, when the curvature of a planet may not be ignored. All global and quasi-global medium- and low-resolution DEMs (e. g., SRTM1, ASTER GDEM, SRTM30_PLUS, GTOPO30) are based on grids of the second kind.

For plane square grids, there are several algorithms for calculation of local variables, such as slope gradient and curvatures. These algorithms are based on approximation of the partial derivatives of elevation by finite differences (Young, 1978; Evans, 1979; Zevenbergen & Thorne, 1987; Shary, 1995; Florinsky, 2009; Minár et al., 2013). There is also a family of methods for derivation of nonlocal variables, e. g. catchment and dispersive areas. Such methods are based on flow-routing logical procedures. They can be grouped into three main types: (1) eight-node single-flow direction (D8) algorithms; (2) multiple-flow direction (D$\infty$) algorithms; and (3) D8-D$\infty$ hybrid approaches (O'Callaghan & Mark, 1984; Martz & de Jong, 1988; Freeman, 1991; Quinn, Beven, Chevallier, & Planchon, 1991; Tarboton, 1997; Wilson, Aggett, Deng, & Lam, 2008; Orlandini & Moretti, 2009; Qin, Bao, Zhu, Hu, & Qin, 2013). Computation of combined variables, such as topographic and stream power indices, is usually based on consecutive application of two algorithms for nonlocal and local variables.

For spheroidal equal angular grids, there is a method for calculation of local morphometric variables (Florinsky, 1998; Florinsky, 2012, §4.3) and an approach for adaptation of any flow-routing algorithm to the geometry of a spheroidal equal angular grid (Florinsky, 2012, pp. 60–61).

Experienced users are aware that methods and algorithms intended for plane square-gridded DEMs should not be directly applied to spheroidal equal angular DEMs. This is because these grids have principally different geometry (Figure 1): in spheroidal equal angular grids, a grid/cell size (measured in linear units) depends on the latitude.

There are only two correct options to handle spheroidal equal angular DEMs. First, one can re-project and interpolate a spheroidal equal angular DEM into a plane square-gridded DEM, and then apply methods for plane square grids to the re-projected DEM. Second, one can directly utilize algorithms specially developed for spheroidal equal angular grids.

For example, re-projection and interpolation of the GTOPO30 data have been performed to compute quasi-global models of slope gradient (*G*), catchment area (*CA*), topographic index (*TI*), and some other morphometric attributes for HYDRO1k, the quasi-global hydrographic database (Verdin & Greenlee, 1998; USGS, 2000). Direct treatment of global spheroidal equal angular DEMs of the Earth, Mars, Venus, and the Moon has been conducted to calculate a set of global models of local and nonlocal morphometric variables for these planetary bodies (Florinsky, 2008a, b; Florinsky & Filippov, 2016). A global model of *TI* has been also computed for Mars (Florinsky, 2008b).

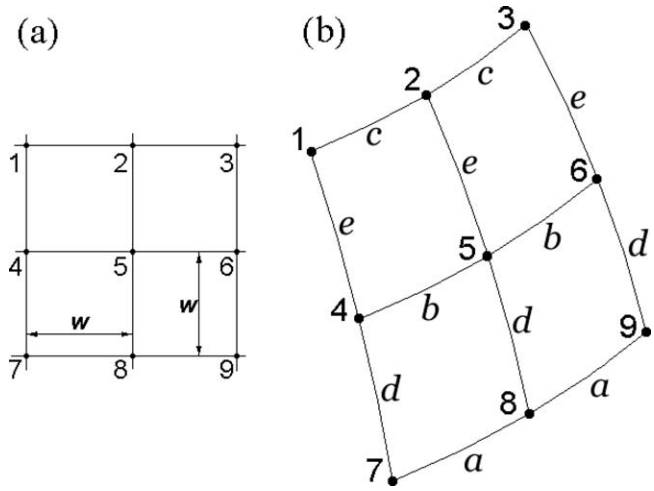


**FIGURE 2** Moving windows used to calculate local morphometric variables: (a) A 3 × 3 plane square-gridded window; *w* is a grid spacing (m); and (b) A 3 × 3 spheroidal equal angular window, *a*, *b*, *c*, *d*, and *e* are linear sizes (m) of moving window elements. 1, . . ., 9 are numbers of the window nodes

At the same time, Guth (2006) has presented a comparison of twelve morphometric parameters (including *G* and some curvatures) for the US, directly derived from two spheroidal equal angular DEMs (SRTM and NED) by methods intended for plane square grids. Marthews, Dadson, Lehner, Abele, and Gedney, (2015) have recently reported the preparation of quasi-global models of *CA* and *TI* using HydroSHEDS, the SRTM3-derived hydrographic database (Lehner, 2013). The computation of *CA* and *TI* were performed directly on the spheroidal equal angular grid using methods intended for plane square grids, ignoring the dependence of cell sizes on the latitude.

Thus, it seems appropriate to consider once again the specifity of morphometric treatment of spheroidal equal angular DEMs. This article, first, demonstrates possibilities of direct calculation of local, nonlocal, and combined morphometric variables from spheroidal equal angular DEMs exemplified by *G*, *CA*, and *TI*. Second, the article shows computational errors when algorithms for plane square-gridded DEMs are unreasonably applied to spheroidal equal angular DEMs to estimate these morphometric variables.

## 2 | METHODS

### 2.1 | Local morphometric variables

Slope gradient is an angle between the tangential and horizontal planes at a given point of the topographic surface. *G* is estimated by the following formula (Shary et al., 2002):

$$G=\arctan\sqrt{p^2+q^2} \tag{1}$$

where *p* and *q* are the first partial derivatives of elevation

$$p=\frac{\partial z}{\partial x},\quad q=\frac{\partial z}{\partial y} \tag{2}$$

For the case of a plane square grid, *p* and *q* can be estimated, for example, by the Evans–Young method (Young 1978; Evans 1979):

$$p=\frac{z_3+z_6+z_9-z_1-z_4-z_7}{6w}, \tag{3}$$

$$q=\frac{z_1+z_2+z_3-z_7-z_8-z_9}{6w}, \tag{4}$$

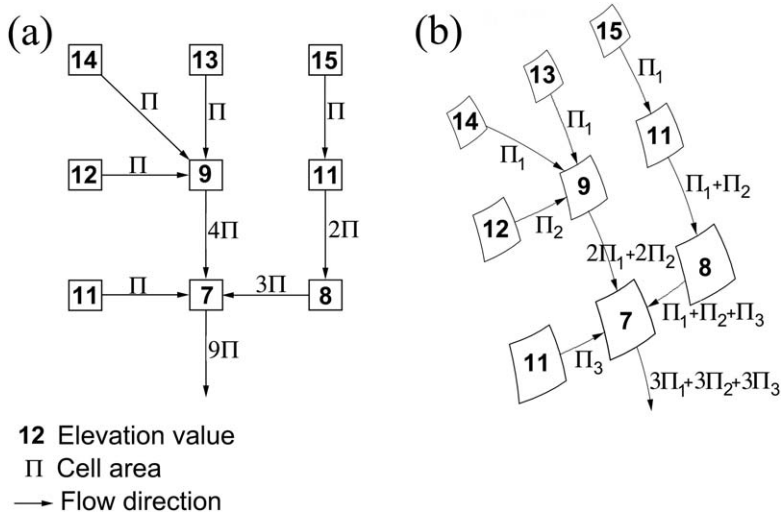


**FIGURE 3** Schemes for the D8 flow routing algorithms: (a) Plane square grid; and (b) Spheroidal equal angular grid. $\Pi_1$, $\Pi_2$, and $\Pi_3$ are cell unit areas at different latitudes

where $z_1, \ldots, z_9$ are elevation values in the nodes of a 3 × 3 moving window and $w$ is the cell size (Figure 2a). Moving the window along a plane square-gridded DEM, one can calculate $p$ and $q$ values (and so $G$ values) for all points of the DEM, except for boundary rows and columns.

For the case of a spheroidal equal angular grid, $p$ and $q$ are estimated by the following expressions (Florinsky, 1998; Florinsky, 2012, § 4.3):

$$p=\frac{a^2cd(d+e)(z_3-z_1)+b\left(a^2d^2+c^2e^2\right)(z_6-z_4)+ac^2e(d+e)(z_9-z_7)}{2\left[a^2c^2(d+e)^2+b^2\left(a^2d^2+c^2e^2\right)\right]}, \tag{5}$$

$$\begin{aligned} q=\frac{1}{3de(d+e)(a^4+b^4+c^4)}\times\{&\left[d^2\left(a^4+b^4+b^2c^2\right)+c^2e^2\left(a^2-b^2\right)\right](z_1+z_3)\\ &-\left[d^2\left(a^4+c^4+b^2c^2\right)-e^2\left(a^4+c^4+a^2b^2\right)\right](z_4+z_6)\\ &-\left[e^2\left(b^4+c^4+a^2b^2\right)-a^2d^2\left(b^2-c^2\right)\right](z_7+z_9)\\ &+d^2\left[b^4(z_2-3z_5)+c^4(3z_2-z_5)+\left(a^4-2b^2c^2\right)(z_2-z_5)\right]\\ &+e^2\left[a^4(z_5-3z_8)+b^4(3z_5-z_8)+\left(c^4-2a^2b^2\right)(z_5-z_8)\right]\\ &-2\left[a^2d^2\left(b^2-c^2\right)z_8+c^2e^2\left(a^2-b^2\right)z_2\right]\} \end{aligned} \tag{6}$$

where $z_1, \ldots, z_9$ are elevation values at the nodes of a 3 × 3 spheroidal equal angular moving window; $a$, $b$, $c$, $d$, and $e$ are linear sizes of the elements of the moving window (Figure 2b). Moving the window along a spheroidal equal angular DEM, one can calculate $p$ and $q$ values (and so $G$ values) for all points of the DEM, except for boundary rows and columns.

Values of $a$, $b$, $c$, $d$, and $e$ depend on the latitude. Since geographic coordinates are known for every point of a spheroidal equal angular grid, so $a$, $b$, $c$, $d$, and $e$ are easily calculated by formulas for the solution of the inverse geodetic problem for short distances (Morozov 1979, pp. 178–179), as described below.

On an ellipsoid of revolution, the distance $L$ (measured in meters) between two points ($\varphi_1$, $\lambda_1$) and ($\varphi_2$, $\lambda_2$), where $\varphi$ is latitude and $\lambda$ is longitude, can be found by the following equation:

$$L=\sqrt{Q^2+P^2}, \tag{7}$$

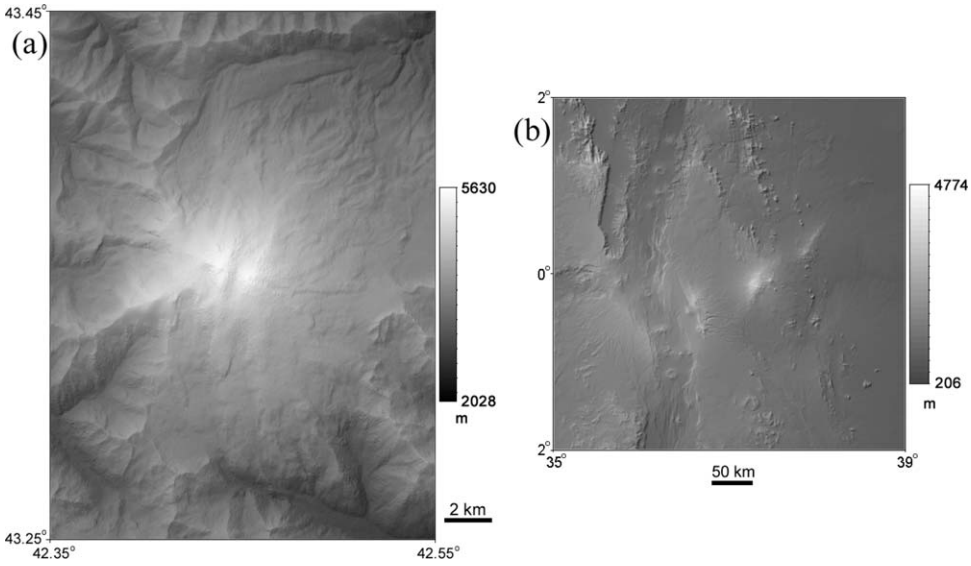


**FIGURE 4** Two areas under study: (a) Mount Elbrus; and (b) The central and western regions of Kenya. Combinations of elevation and hill-shaded maps (Lambertian models; solar azimuth and solar elevation angles are 315° and 45°, respectively)

$$Q=\Theta M_m\left[1-\left(E'^2-2\eta_m^2\right)\frac{\Theta^2}{8}-\left(1+\eta_m^2\right)\frac{(\Lambda\cos\varphi_m)^2}{12}-\frac{(\Lambda\sin\varphi_m)^2}{8}\right] \tag{8}$$

$$P=\Lambda\cos\varphi_m N_m\left[1+\left(1-9E'^2+8\eta_m^2\right)\frac{\Theta^2}{24}-\frac{(\Lambda\sin\varphi_m)^2}{24}\right], \tag{9}$$

$$\Theta=\varphi_2-\varphi_1 \text{ (measured in radians)} \tag{10}$$

$$\Lambda=\lambda_2-\lambda_1 \text{ (measured in radians)} \tag{11}$$

$$\varphi_m=\frac{1}{2}(\varphi_1+\varphi_2) \tag{12}$$

$$E'=\frac{\sqrt{A^2-B^2}}{B} \tag{13}$$

and $E'$ is the second eccentricity, and $A$ and $B$ are semi-major and semi-minor axes of the ellipsoid of revolution, respectively, and:

$$\eta_m^2=E'^2\cos^2\varphi_m \tag{14}$$

$$N_m=\frac{C}{\sqrt{1+\eta_m^2}} \tag{15}$$

$$C=\frac{A^2}{B} \tag{16}$$

$$M_m=\frac{N_m}{1+\eta_m^2} \tag{17}$$

Alternative formulas to solve the inverse geodetic problem can be found elsewhere (Sodano, 1965; Vincenty, 1975; Bowring, 1996).

## 2.2 | Nonlocal morphometric variables

Catchment area is an area of a closed figure formed by a contour segment at a given point of the topographic surface and two flow lines coming from upslope to the contour segment ends (Speight, 1974).

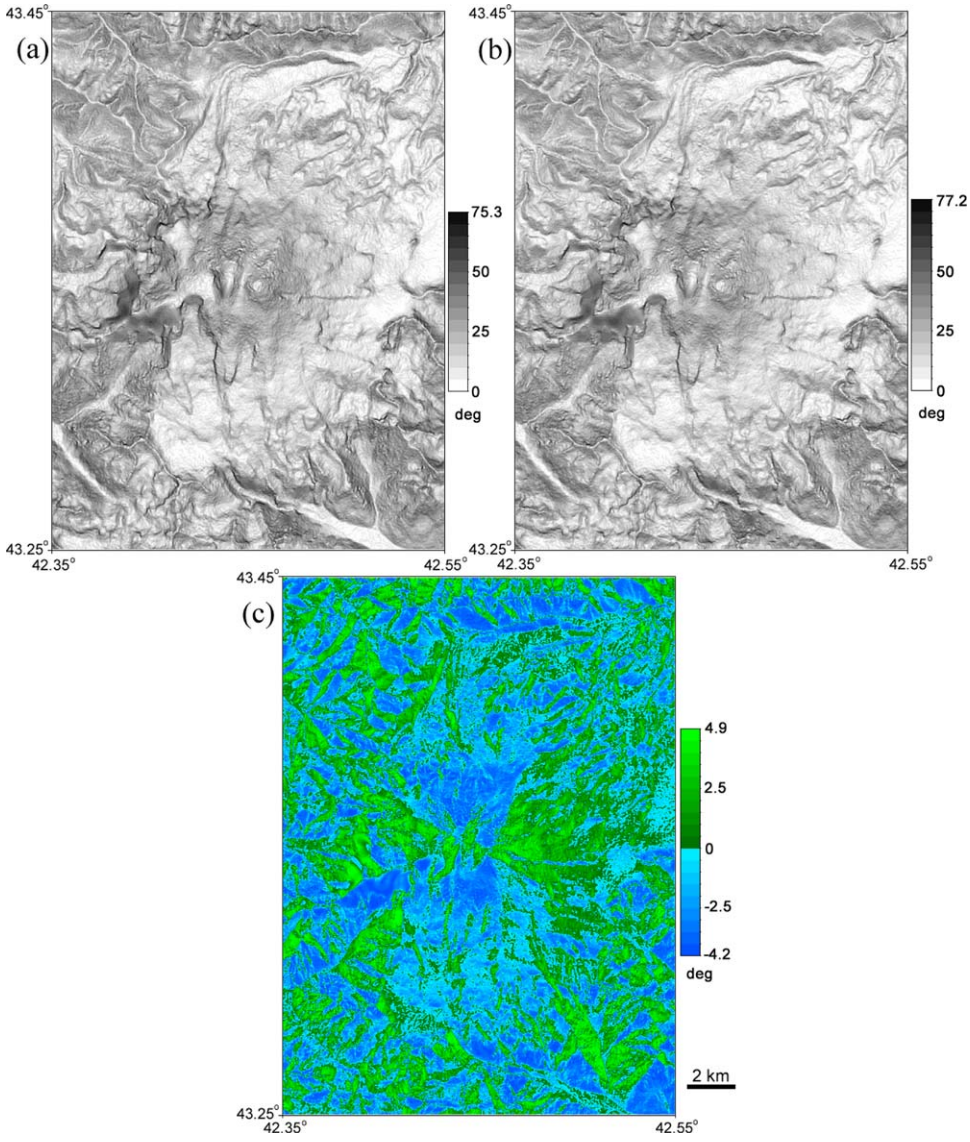


**FIGURE 5** Mount Elbrus, slope gradient: (a) The *G* model derived by the method for spheroidal equal angular grids; (b) The *G* model derived by the method for plane square grids: and (c) The difference between two *G* models

For the case of a plane square grid, one can estimate *CA*, for example, by the Martz–de Jong method (Martz & de Jong, 1988). As a D8 algorithm, the Martz–de Jong method uses only one of the eight possible directions separated by 45° to model a flow from a given point. The flow direction is determined by estimating a value of *G* to each neighbor of the point; it corresponds to the direction for which *G* is the greatest. *CA* at a downslope point is determined as the number of upslope points, passed by flows to reach this point, multiplied by the cell unit area ($\Pi$) (Figure 3a). It is reasonable to "fill" closed pits or depressions before *CA* calculation. The detailed description of the method as well as its Fortran code can be found elsewhere (Martz & de Jong, 1988).

For the case of a spheroidal equal angular grid, *G* values are estimated as described above (Section 2.1). $\Pi$ depends on the latitude (Figure 3b) and can be estimated by the following expression (Morozov, 1979, p. 34).

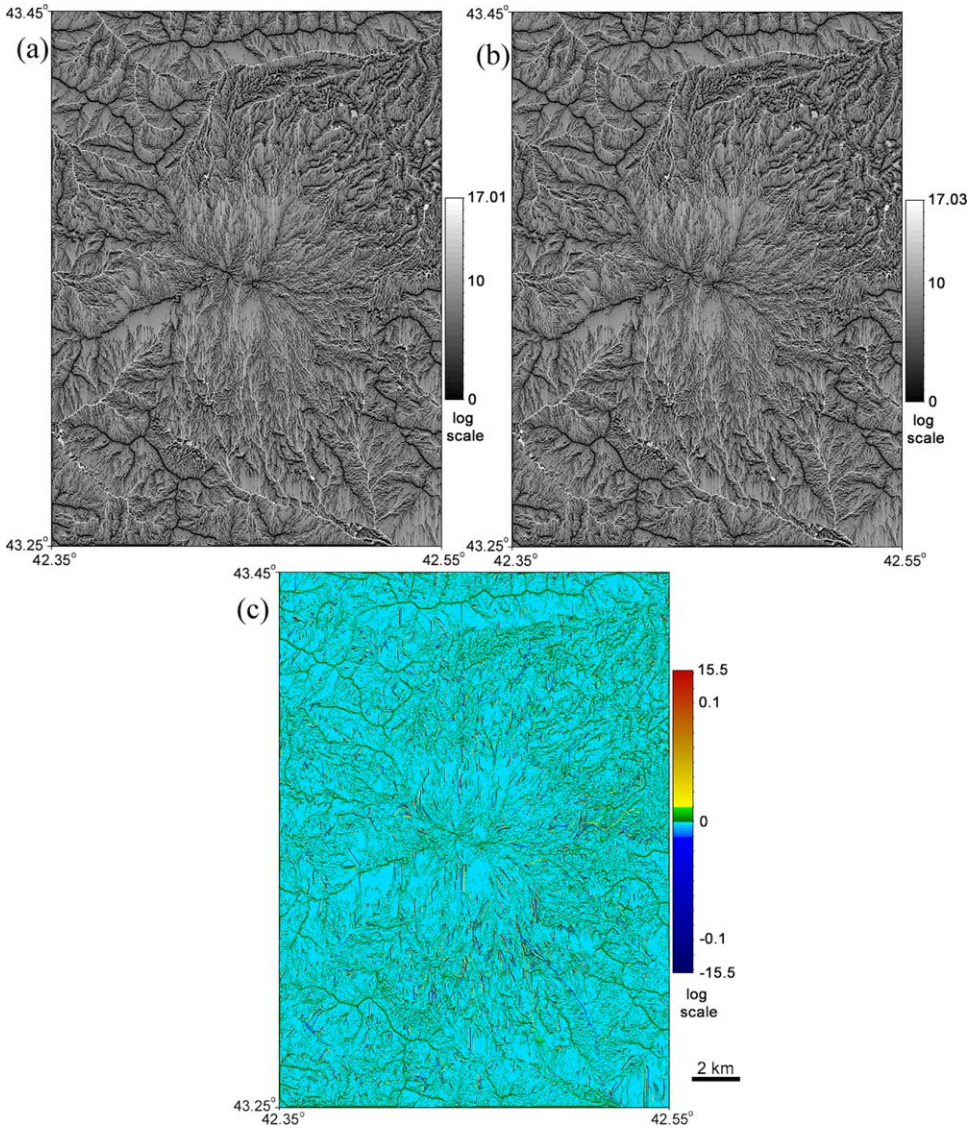


**FIGURE 6** Mount Elbrus, catchment area: (a) The *CA* model derived by the method for spheroidal equal angular grids; (b) The *CA* model derived by the method for plane square grids; and (c) The difference between two *CA* models

$$\Pi = B^2(\lambda_2 - \lambda_1)\left|\sin\varphi + \frac{2}{3}E^2\sin^3\varphi + \frac{3}{5}E^4\sin^5\varphi + \frac{4}{7}E^6\sin^7\varphi + \ldots\right|_{\varphi_1}^{\varphi_2} \tag{18}$$

where $E$ is the first eccentricity of an ellipsoid of revolution, as reported below.

$$E = \frac{\sqrt{A^2 - B^2}}{A} \tag{19}$$

Such an approach allows adapting any flow-routing algorithm to the geometry of a spheroidal equal angular grid (Florinsky, 2012, pp. 60–61).

A wide dynamic range characterizes *CA*. To avoid loss of information on spatial distribution of *CA* values in mapping, there is a need to apply a logarithmic transform of *CA* using the following expression:

$$CA' = \ln(1 + CA). \tag{20}$$

The term 1 is used to avoid negative values of $CA'$.

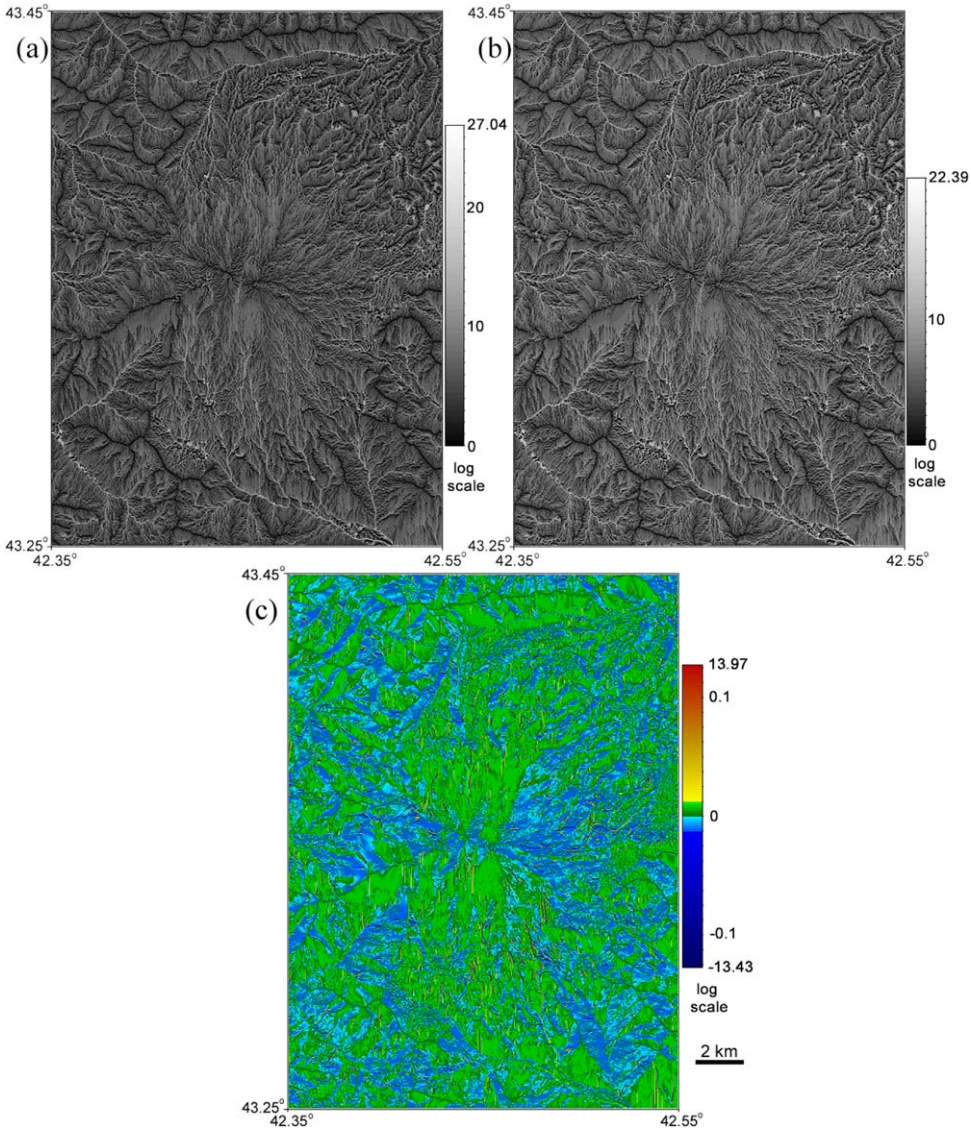


**FIGURE 7** Mount Elbrus, topographic index: (a) The *TI* model derived by the method for spheroidal equal angular grids; (b) The *TI* model derived by the method for plane square grids; and (c) The difference between two *TI* models

## 2.3 | Combined morphometric variables

Topographic index is usually estimated by the following equation (Beven & Kirkby, 1979):

$$TI = \ln\left(1 + CA/\left(10^{-3} + \tan G\right)\right). \tag{21}$$

Due to the term 1 in Eq. (21) *TI* is a nonnegative variable. The term $10^{-3}$ is used to avoid division by zero for the case of horizontal planes. *TI* is a dimensionless variable; it is used as a measure of the extent of flow accumulation in TOPMODEL, a conceptual distributed hydrological modeling (Beven & Kirkby, 1979; Quinn, Beven, & Lamb, 1995).

*TI* derivation includes: (1) calculations of *CA* and *G* by related methods described above, and (2) subsequent arithmetic combination of two digital terrain models (DTMs) obtained. It is obvious that selection of both methods depends strongly on the DEM grid type. It would be incorrect to mix methods intended for different grid types, for instance, to calculate *CA* by a method for square grids, while to compute *G* by a method for spheroidal equal angular grids (or, vice versa).

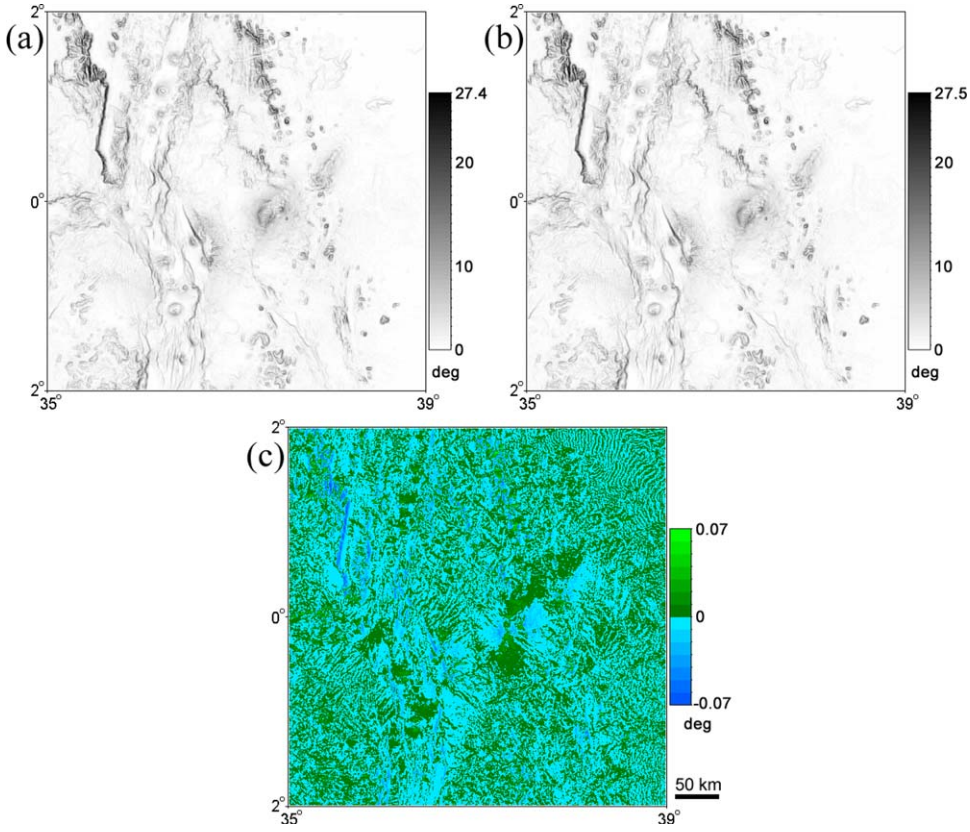


**FIGURE 8** Kenya, slope gradient: (a) The *G* model derived by the method for spheroidal equal angular grids; (b) The *G* model derived by the method for plane square grids; and (c) The difference between two *G* models

## 3 | MATERIALS AND DATA PROCESSING

The study is exemplified by two DEMs with different resolution: (1) a medium-resolution DEM of a relatively small, high-mountainous area; and (2) a low-resolution DEM of a vast area with diverse topography.

A high-mountainous area is represented by Mount Elbrus in the North Caucasus, Russia (Figure 4a). The area is located between 43.25° and 43.45° N, and 42.35° and 42.55° E (the area size is 12′ × 12′). A spheroidal equal angular DEM was extracted from the quasi-global SRTM1 DEM (Farr et al., 2007; USGS, 2015). The DEM includes 519,841 points (the matrix 721 × 721); the grid spacing is 1″.

A vast region with diverse topography is represented by the central and western regions of Kenya, including a portion of the Great Rift Valley and central Kenyan highlands (Figure 4b). The area is located between 2° S and 2° N, and 35° and 39° E (the area size is 4° × 4°). A spheroidal equal angular DEM was extracted from the global DEM SRTM30_PLUS (Becker et al., 2009; Sandwell et al., 2008). The DEM includes 230,880 points (the matrix 480 × 481); the grid spacing is 30″.

First, to demonstrate possibilities of direct calculation of morphometric variables from spheroidal equal angular DEMs, digital models of *G*, *CA*, and *TI* were derived from these two DEMs by the methods intended for spheroidal equal angular grids (described in Section 2). Second, to show computational errors of unreasonable application of algorithms for square grids to spheroidal equal angular DEMs, digital models of *G*, *CA*, and *TI* were derived from these two DEMs by the methods intended for square grids (described in Section 2) without preliminary re-projection and interpolation of the DEMs.

In both cases, the WGS-84 ellipsoid parameters were used. In calculations with the methods for square grids, an average of the linear sizes of a cell at the mean latitude of a study area was utilized as a constant grid size. In particular,

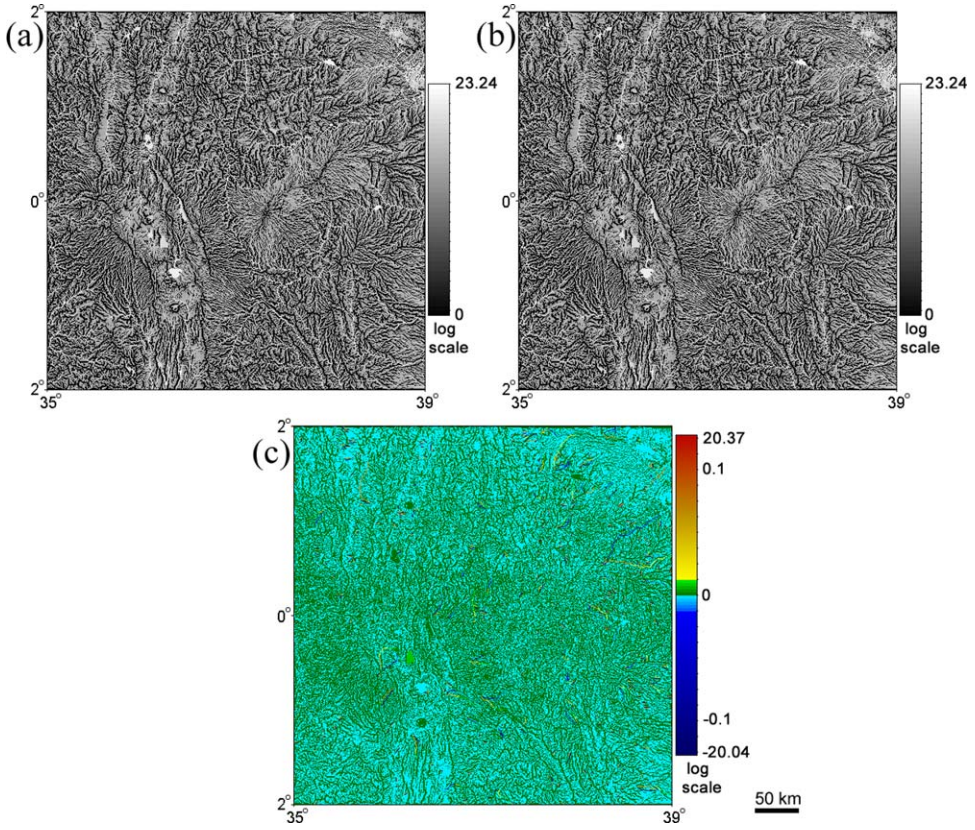


**FIGURE 9** Kenya, catchment area: (a) The *CA* model derived by the method for spheroidal equal angular grids; (b) The *CA* model derived by the method for plane square grids; and (c) The difference between two *CA* models

for the Elbrusian DEM, the linear sizes of the 1″ × 1″ cell are 30.86 m × 22.52 m at the mean latitude, 43.35° N. For the Kenyan DEM, the linear sizes of the 30″ × 30″ cell are 921.45 m × 927.66 m at the mean latitude, the equator. Thus, 26.69 m and 924.55 m were utilized as the constant grid sizes for the Elbrusian and Kenyan DEMs, respectively.

To evaluate computational errors in DTMs derived by the methods for plane square grids, three procedures were carried out. First, simple differences between DTM pairs were estimated (a DTM derived by a method for plane square grids was subtracted from a DTM derived by a method for spheroidal equal angular grids). Second, descriptive statistics were determined for all DTMs. Third, a pairwise comparison of the DTMs calculated by the methods for spheroidal equal angular grids and plane square grids was performed using the two-sample Kolmogorov–Smirnov (K–S) test (Daniel, 2000, ch. 8). Samples were extracted from each DTM. For the Elbrusian DTMs, the sample size was 4,900 points (the matrix 70 × 70 with the grid spacing of 10″). For the Kenyan DTMs, the sample size was 2,209 points (the matrix 47 × 47 with the grid spacing of 5′).

DTM processing and mapping was conducted with the software LandLord (Florinsky, 2012, pp. 315–316). Statistical analysis was carried out with the software Statgraphics Plus 3.0 (© Statistical Graphics Corp. 1994–1997).

## 4 | RESULTS

Figures 5a, 6a, 7a, 8a, 9a, and 10a demonstrate models of *G*, *CA*, and *TI* derived from the Elbrusian and Kenyan DEMs by the methods for spheroidal equal angular grids. Figures 5b, 6b, 7b, 8b, 9b, and 10b represent models of *G*, *CA*, and *TI* derived by the square-grid methods. Tables 1 and 2 summarize statistics for these models.

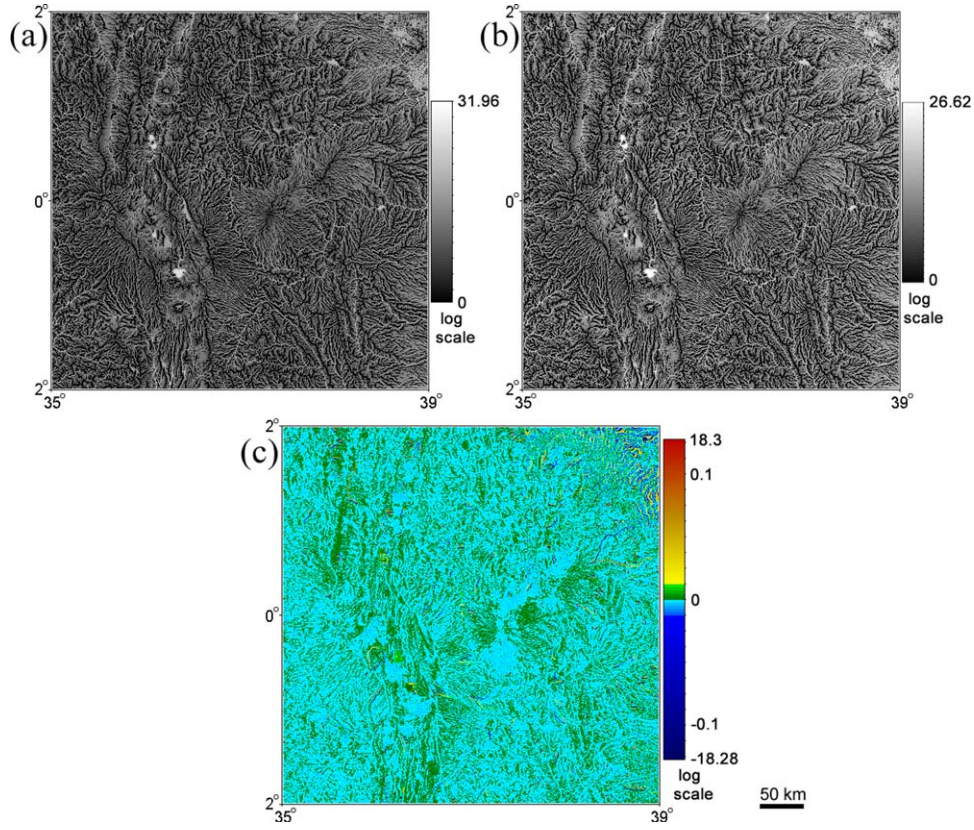


**FIGURE 10** Kenya, topographic index: (a) The *TI* model derived by the method for spheroidal equal angular grids; (b) The *TI* model derived by the method for plane square grids; and (c) The difference between two *TI* models

Visually, pairs of maps obtained by the methods for different grid types seem to be almost identical (cf. Figures 5a with 5b, 6a with 6b, 8a with 8b, and 9a with 9b). Although we used large sample sizes, descriptive statistics (Tables 1 and 2) do not provide information on differences between the models: presented statistics are very similar. However, in some cases there are clear differences in the maximal values of *G* and *TI* (cf. legends in Figures 5a with 5b, 7a with 7b, and 10a with 10b).

Figures 5c, 6c, 7c, 8c, 9c, and 10c represent differences between pairs of DTMs derived by the methods for different grid types. In fact, these differences are computational errors due to unreasonable application of the square-grid

**TABLE 1** Statistics for the Elbrusian DTMs derived by the methods for spheroidal equal angular (SEA) and plane square (PS) grids

| Statistics | *G* | | *CA* | | *TI* | |
|---|---|---|---|---|---|---|
| | SEA | PS | SEA | PS | SEA | PS |
| Minimum | 0.424 | 0.344 | 0.000 | 0.000 | 0.000 | 0.000 |
| Maximum | 66.098 | 63.723 | 16.740 | 16.767 | 16.669 | 16.921 |
| Average | 22.736 | 23.055 | 6.902 | 6.904 | 5.061 | 5.041 |
| Standard deviation | 11.382 | 11.683 | 3.802 | 3.818 | 3.106 | 3.109 |
| Standardized skewness | 8.728 | 9.106 | −22.832 | −22.705 | −3.881 | −3.487 |
| Standardized kurtosis | −4.916 | −5.815 | −3.192 | −3.490 | −1.123 | −0.940 |

**TABLE 2** Statistics for the Kenyan DTMs derived by the methods for spheroidal equal angular (SEA) and plane square (PS) grids

| Statistics | *G* | | *CA* | | *TI* | |
|---|---|---|---|---|---|---|
| | SEA | PS | SEA | PS | SEA | PS |
| Minimum | 0.000 | 0.000 | 0.000 | 0.000 | 0.000 | 0.000 |
| Maximum | 23.272 | 23.343 | 22.815 | 22.816 | 26.620 | 26.620 |
| Average | 1.898 | 1.899 | 9.342 | 9.335 | 7.671 | 7.663 |
| Standard deviation | 2.457 | 2.460 | 7.893 | 7.886 | 6.691 | 6.683 |
| Standardized skewness | 63.017 | 63.104 | −4.684 | −4.700 | −0.864 | −0.888 |
| Standardized kurtosis | 145.872 | 146.375 | −16.590 | −16.598 | −14.309 | −14.321 |

methods. The errors have both positive and negative values, that is, such use of the square-grid methods leads to both under- and overestimation of *G*, *CA*, and *TI* values.

It is clearly seen that the amplitudes of computational errors for *CA* and *TI* are comparable with the ranges of *CA* and *TI* values (cf. legends in Figs. 6c with 6a, 7c with 7a, 9c with 9a, and 10c with 10a). However, high errors are relatively rare against the background of very small errors (to contrast this, we used a non-uniform colour scale for Figures 6c, 7c, 9c and 10c). Lowest absolute values of *CA* errors are typical for crests and slopes (dark green lines and light blue areas, correspondingly), while highest absolute values of *CA* errors can be found in some thalwegs (yellow and dark blue lines). This was expected because a gradual accumulation of *CA* errors occurs from up- to downslopes. For *G*, computational errors are less expressed (cf. legends in Figure 5c and 5a), especially for the equatorial zone where the linear sizes of spheroidal trapezium cells differ slightly from a square (cf. legends in Figure 8c and 8a). High absolute values of *G* errors are typical for steep slopes.

According to the K–S test, if $D_n > D_{0.05}$, one can assume that there is a statistically significant difference between the two distributions at the 95% confidence level. $D_{0.05} = 0.027$ for $n = 4900$, and $D_{0.05} = 0.041$ for $n = 2209$. Based on the K–S test results (Table 3), *CA* and *TI* models calculated by the methods for spheroidal equal angular grids are statistically different from those calculated by the square-grid methods. At the same time, there are no statistical differences between *G* models calculated by methods intended for different grid types. However, although such a statistical interpretation may be accepted for the equatorial zone where the calculation error is ±0.07° (Figure 8c), it is hard to believe that one would ignore the error in *G* calculation ranging from −4.2° to 4.9° (Figure 5c).

**TABLE 3** Statistics for the differences between the pairs of DTMs derived by the methods for spheroidal equal angular and plane square grids

| Statistics | The Elbrusian DTMs | | | The Kenyan DTMs | | |
|---|---|---|---|---|---|---|
| | G | CA | TI | G | CA | TI |
| Minimum | −4.171 | −10.728 | −9.309 | −0.071 | −14.353 | −11.651 |
| Maximum | 4.890 | 9.252 | 8.085 | 0.034 | 16.603 | 13.949 |
| Average | −0.319 | −0.002 | 0.019 | −0.001 | 0.007 | 0.007 |
| Standard deviation | 2.184 | 0.627 | 0.518 | 0.007 | 0.781 | 0.654 |
| K–S test | | | | | | |
| $D_n$ | 0.020 | 0.202 | 0.202 | 0.003 | 0.406 | 0.406 |
| K–S | 1.000 | 10.021 | 10.021 | 0.105 | 13.495 | 13.495 |
| P value | 0.271 | 0.00 | 0.00 | 1.00 | 0.00 | 0.00 |

## 5 | DISCUSSION

Mathematically, square-grid methods can be considered "an approximation" of spheroidal approaches for the equatorial zone only, where the shape of spheroidal trapezoidal cells is relatively close to a square. The farther from the equator, the stronger the shape of a DEM cell differs from a square. It is obvious that discussed computational errors increase with increasing distance from the equator. It is also quite evident that the lower the resolution of a spheroidal equal angular DEM (that is, the larger a DEM cell size), the higher the absolute values of the discussed errors. The results suggest that higher errors may be obtained for steep slopes in mountainous terrain.

It is impossible to correct results if methods for square-grid DEMs were used to treat a spheroidal equal angular DEM. The correct way is to use spheroidal approaches. In general, square-grid methods should be applied to treat square-gridded DEMs of high- and medium-resolution for relatively small areas. Spheroidal approaches should be employed to treat spheroidal equal-angular DEMs of any resolution describing the globe or vast territories.

This study analyzed one square-grid method for the calculation of local morphometric variables, and one square-grid algorithm for derivation of nonlocal attributes. At the same time, at a plane square grid, $p$ and $q$ (and so $G$) can be also estimated by other finite-difference methods (Zevenbergen & Thorne, 1987; Shary, 1995; Florinsky, 2009; Minár et al., 2013), while $CA$ can be derived by other flow-routing algorithms (O'Callaghan & Mark, 1984; Freeman, 1991; Quinn et al., 1991; Tarboton, 1997). It is obvious that their application would result in somewhat different models of $G$, $CA$, and $TI$ (and so somewhat different computational errors). However, for the purposes of our study, it does not matter exactly which square-grid method is used to process a spheroidal equal angular DEM, because any such use is incorrect.

## 6 | CONCLUSIONS

The results of the study show that application of square-grid methods to treat spheroidal equal angular DEMs leads to substantial computational errors in models of local, nonlocal, and combined morphometric variables. The direct use of square-grid methods at spheroidal grids is absolutely unreasonable because there are methods specially designed for such situations. This article can help users to distinguish between different types of DEM grids and to choose a correct geomorphometric approach according to a particular grid type.

### ACKNOWLEDGMENTS

The study was supported by the Russian Foundation for Basic Research grant 15-07-02484.

### REFERENCES

Becker, J. J., Sandwell, D, T., Smith, W. H. F., Braud, J., Binder, B., Depner, J., . . ., & Weatherall, P. (2009). Global bathymetry and elevation data at 30 arc seconds resolution: SRTM30_PLUS. *Marine Geodesy*, *32*, 355–371.

Beven, K. J., & Kirkby, M. J. (1979). A physically-based variable contributing area model of basin hydrology. *Hydrological Science Bulletin*, *24*, 43–69.

Bowring, B. R. (1981). The direct and inverse problems for short geodesic lines on the ellipsoid. *Surveying & Mapping*, *41*, 135–141.

Brocklehurst, S. H. (2010). Tectonics and geomorphology. *Progress in Physical Geography*, *34*, 357–383.

Daniel, W. W. (2000). *Applied nonparametric statistics* (2nd Ed). Belmont, CA: Cengage Learning.

Deng, Y. (2007). New trends in digital terrain analysis: Landform definition, representation, and classification. *Progress in Physical Geography*, *31*, 405–419.

Evans, I. S. (1979). *Statistical characterization of altitude matrices by computer: An integrated system of terrain analysis and slope mapping*. Durham, UK, University of Durham Final Report on Grant DA-ERO-591-73-G0040.

Farr, T. G., Rosen, P. A., Caro, E., Crippen, R., Duren, R., Hensley, S., . . ., & Alsdorf, D. (2007). The Shuttle Radar Topography Mission. *Reviews of Geophysics*, *45*, RG2004.

Florinsky, I. V. (1998). Derivation of topographic variables from a digital elevation model given by a spheroidal trapezoidal grid. *International Journal of Geographical Information Science*, *12*, 829–852.

Florinsky, I. V. (2008a). Global lineaments: Application of digital terrain modelling. In Q. Zhou, B. Lees, & G.-A. Tang (Eds.), *Advances in digital terrain analysis* (pp. 365–382). Berlin, Germany: Springer.

Florinsky, I. V. (2008b). Global morphometric maps of Mars, Venus, and the Moon. In A. Moore & I. Drecki (Eds.), *Geospatial vision: New dimensions in cartography* (pp. 171–192). Berlin, Germany: Springer.

Florinsky, I. V. (2009). Computation of the third-order partial derivatives from a digital elevation model. *International Journal of Geographical Information Science*, *23*, 213–231.

Florinsky, I. V. (2012). *Digital terrain analysis in soil science and geology*. Amsterdam, the Netherlands: Academic Press.

Florinsky, I. V., & Filippov, S. V. (2016). Virtual morphometric globes: Applying the software Blender. Keldysh Institute Preprints, 37 (in Russian, with English abstract).

Franklin, J. (1995). Predictive vegetation mapping: Geographic modelling of biospatial patterns in relation to environmental gradients. *Progress in Physical Geography*, *19*, 474–499.

Freeman, T. G. (1991). Calculating catchment area with divergent flow based on a regular grid. *Computers & Geosciences*, *17*, 413–422.

Guth, P. L. (2006). Geomorphometry from SRTM: Comparison *to NED*. *Photogrammetric Engineering & Remote Sensing*, *72*, 269–277.

Hengl, T., & Reuter, H. I. (Eds.) (2009). *Geomorphometry: Concepts, software, applications*. Amsterdam, the Netherlands: Elsevier.

Lehner, B. (2013). *HydroSHEDS Technical Documentation. Version 1.2*. Washington, DC: World Wildlife Fund.

Li, Z., Zhu, Q., & Gold, C. (2005). *Digital terrain modeling: Principles and methodology*. Boca Raton, FL: CRC Press.

Marthews, T. R., Dadson, S. J., Lehner, B., Abele, S., & Gedney, N. (2015). High-resolution global topographic index values for use in large-scale hydrological modelling. *Hydrology & Earth System Sciences*, *19*, 91–104.

Martz, L. W., & de Jong, E. (1988). CATCH: A Fortran program for measuring catchment area from digital elevation models. *Computers & Geosciences*, *14*, 627–640.

Minár, J., Jenčo, M., Evans, I. S., Minár, J. Jr., Kadlec, M., Krcho, J., . . ., & Benová, A. (2013). Third-order geomorphometric variables (derivatives): Definition, computation and utilization of changes of curvatures. *International Journal of Geographical Information Science*, *27*, 1381–1402.

Moore, I. D., Grayson, R. B., & Ladson, A. R. (1991). Digital terrain modelling: A review of hydrological, geomorphological and biological applications. *Hydrological Processes*, *5*, 3–30.

Morozov, V. P. (1979). *A course in spheroidal geodesy* (2nd Ed.). Moscow, Russia: Nedra (in Russian).

O'Callaghan, J. F., & Mark, D. M. (1984). The extraction of drainage networks from digital elevation data. *Computer Vision, Graphics, & Image Processing*, *28*, 323–344.

Orlandini, S., & Moretti, G. (2009). Determination of surface flow paths from gridded elevation data. *Water Resources Research*, *45*, W03417.

Qin, C.-Z., Bao, L.-L., Zhu, A.-X., Hu, X.-M., & Qin, B. (2013). Artificial surfaces simulating complex terrain types for evaluating grid-based flow direction algorithms. *International Journal of Geographical Information Science*, *27*, 1055–1072.

Quinn, P. F., Beven, K. J., Chevallier, P., & Planchon, O. (1991). The prediction of hillslope flow paths for distributed modelling using digital terrain models. *Hydrological Processes*, *5*, 59–80.

Quinn, P., Beven, K., & Lamb, R. (1995). The ln(a/tan β) index: How to calculate it and how to use it within the TOPMODEL framework. *Hydrological Processes*, *9*, 161–182.

Sandwell, D. T., Smith, W. H. F., & Becker, J. J. (2008). *SRTM30_PLUS V11*. Retrieved from ftp://topex.ucsd.edu/pub/srtm30_plus/

Shary, P. A. (1995). Land surface in gravity points classification by a complete system of curvatures. *Mathematical Geology*, *27*, 373–390.

Shary, P. A., Sharaya, L. S., & Mitusov, A. V. (2002). Fundamental quantitative methods of land surface analysis. *Geoderma*, *107*, 1–32.

Sodano, E. M. (1965). General non-iterative solution of the inverse and direct geodetic problems. *Bulletin Géodésique*, *75*, 69–89.

Speight, J. G. (1974). A parametric approach to landform regions. In E. H. Brown & R. S. Waters (Eds.), *Progress in geomorphology: Papers in honour of D. L. Linton* (pp. 213–230). London, UK: Institute of British Geographers.

Tarboton, D. G. (1997). A new method for the determination of flow directions and upslope areas in grid digital elevation models. *Water Resources Research*, *33*, 309–319.

USGS. (2000). *HYDRO1k Elevation Derivative Database*. Retrieved from https://lta.cr.usgs.gov/HYDRO1K

USGS. (2015). *Earth Explorer*. Retrieved from http://earthexplorer.usgs.gov

Verdin, K. L., & Greenlee S. K. (1998). *HYDRO1k documentation*. Sioux Fall, SD: Earth Resources Observation & Science (EROS) Center, U.S. Geological Survey.

Vincenty, T. (1975). Direct and inverse solutions of geodesics on the ellipsoid with application of nested equations. *Survey Review*, *23*, 88–93.

Wilson, J. P., & Gallant, J. C. (Eds.) (2000). *Terrain analysis: Principles and applications*. New York, NY: John Wiley & Sons.

Wilson, J. P., Aggett, G., Deng, Y., & Lam, C. S. (2008). Water in the landscape: A review of contemporary flow routing algorithms. In Q. Zhou, B. Lees, & G. A. Tang (Eds.), *Advances in digital terrain analysis* (pp. 213–236). Berlin, Germany: Springer.

Young, M, (1978) *Statistical characterization of altitude matrices by computer. Terrain analysis: program documentation*. Durham, UK: University of Durham, Report No. 5 on Grant DA-ERO-591-73-G0040.

Zevenbergen, L. W., & Thorne, C. R. (1987). Quantitative analysis of land surface topography. *Earth Surface Processes & Landforms*, *12*, 47–56.

**How to cite this article:** Florinsky IV. Spheroidal equal angular DEMs: The specificity of morphometric treatment. *Transactions in GIS*. 2017;21:1115–1129. https://doi.org/10.1111/tgis.12269